Design and Analysis of a Hybrid PV-PEMFC System with MPPT Controller for a Three-Phase Grid-Connected System

Jyotheeswara Reddy K. and Sudhakar N.*

School of Electrical Engineering, Vellore Institute of Technology, Vellore-632014, India
E-mail: jyothireddy.kalvakurthi@gmail.com; nsudhakar@vit.ac.in
**Corresponding Author*

Received 22 February 2018; Accepted 12 June 2018;
Publication 18 July 2018

Abstract

The renewable energy sources (RES) are stochastic in nature and requires an energy storage system to reduce power fluctuations. In this work, a three-phase grid connected hybrid renewable energy system (HRES) is designed with solar PV and fuel cell. A new radial basis function network (RBFN) based maximum power point tracking (MPPT) controller strategy is designed for fuel cell and a fuzzy logic controller (FLC) is used for solar PV to extract the maximum power at different PEMFC temperatures and solar irradiation levels. In addition to this, a high step-up DC-DC boost converter (HSBC) is designed for fuel cell in order to provide high step-up voltage. The proposed hybrid energy system is designed by considering a 1.26kW proton exchange membrane fuel cell (PEMFC) with HSBC and a 950W solar PV system with conventional boost converter. The proposed system is simulated in MATLAB/Simulink platform to analyse the performance of the system.

Keywords: Hybrid renewable energy system, conventional boost converter, high step-up boost converter, MPPT, PV system, PEMFC.

Journal of Green Engineering, Vol. 8_2, 151–176. *River Publishers*
doi: 10.13052/jge1904-4720.823

1 Introduction

Due to the depletion of fossil fuels and increasing energy consumption, the renewable energy sources (RES) are playing an important role in the modern power system [1, 2]. Unfortunately, the renewable energy sources are stochastic in nature and also generates less power compared to the conventional power sources. Hence, integration of multiple reneawable sources is required to generate more reliable power. Integration of two or more renewable energy sources forms a hybrid renewable energy system [HRES] [3]. In addition to renewable sources, a HRES requires a storage system, power converters, AC or DC distribution system and a control system for an efficient load management [4].

Many researchers have focused their studies on hybrid PV and wind energy systems due to their abundant availabilty in nature. Basaran et al. [5] studied the energy management of standalone and grid-connected hybrid PV-wind systems. In [6], Caballero et al. have studied the optimal design of grid-connected hybrid PV-wind system without energy storage unit. Beharvesh et al. [7] studied the effects of various penetration levels of a hybrid PV-wind system on the daily voltage profile. Kumar and Babu [8] have designed a neural network based single MPPT controller for hybrid solar and wind systems. However, the PV and wind energy sources are unpredictable in nature. The output of the PV and wind sources changes with respect to solar irradiation and wind speed respectively [9]. Hence, different energy storage devices such as batteries, supercapacitors or fuel cells are integrated to the HRES. Due to the abundant availabilty of solar energy and high energy density of fuel cell, the combination of PV and fuel cell sources are good options for the HRES [10, 11]. Fuel cells are categorized into different types depending on the type of electrolyte substance. Different types of fuel cells include alkaline fuel cell (AFC), phosphoric acid fuel cell (PAFC), solid oxide fuel cell (SOFC), proton exchange membrane fuel cell (PEMFC) and molten carbonate fuel cell (MCFC) [12]. Among all these types, PEMFC is dominantly using in electrical applications due to its low noise generation, high power density and small size.

Nomenclature

	Abbreviations
PV	Photovoltaic
MPPT	Maximum Power Point Tracking
RES	Renewable Energy sources

HRES	Hybrid Renewable Energy System
PAFC	Phosphoric Acid Fuel Cell
SOFC	Solid Oxide Fuel Cell
AFC	Alkaline Fuel Cell
PEMFC	Proton Exchange Membrane Fuel Cell
MCFC	Molten Carbonate Fuel Cell
P&O	Perturb & Observation
IC	Incremental Conductance
FLC	Fuzzy Logic Controller
SMC	Sliding Mode Controller
PSO	Particle Swarm Optimization
HC	Hysteresis Controller
RBFN	Radial Basis Function Network
HSBC	High Step-up Boost Converter

	Symbols
V_{PV}	PV output voltage
I_{ph}	PV cell phase current
I_D	Diode saturation current
q	Charge of electron
R_S	Series resistances of the PV cell
R_{Sh}	Parallel resistances of the PV cell
K	Boltzmann constant
T	Absolute temperature of PV system
V_{FC}	PEMFC voltage
I_{FC}	PEMFC current
T_{FC}	PEMFC cell temperature
E_{nernst}	Open circuit thermodynamic voltage
V_{act}	Activation overvoltage
V_{ohm}	Ohmic overvoltage
V_{con}	Concentration over voltage
P_{H2}	Hydrogen partial pressure
P_{O2}	Oxygen gas partial pressure

RES requires power electronic converters for the flexible and efficient integration of the sources with the grid. In grid connected system, AC-DC or DC-AC power converters interface the renewable energy sources and energy storage devices to a DC bus, whereas DC-AC power converters transfers

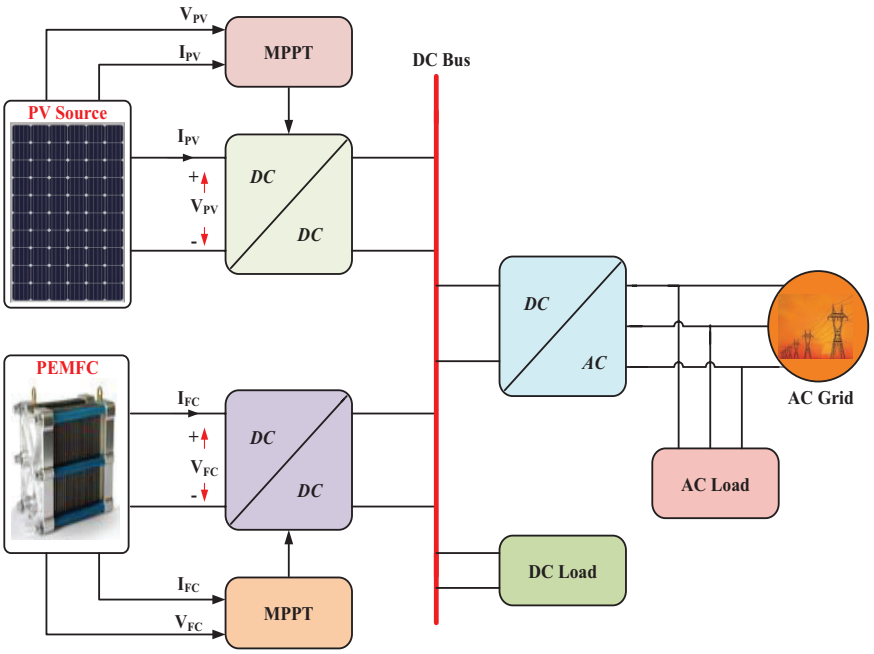

Figure 1 Basic topology of hybrid PV-PEMFC system.

the active and reactive powers to the grid [13]. Figure 1 shows the block diagram of the basic HRES. It consists of energy sources (PV and PEMFC), power converters (DC-DC and DC-AC) and MPPT controllers for energy sources. The V-I characteristics of PV and PEMFC systems are non-linear. The maximum power point (MPP) of the PV system changes with irradiation level and temperature changes, whereas the MPP of the PEMFC changes with respect to change membrane water content and cell temperature [14]. Hence, MPPT controllers are necessary for both PV and PEMFC systems to extract the maximum power. In the literature, some researchers have presented various MPPT techniques for both PV and PEMFC systems such as perturb & observation (P&O) [15, 16], incremental conductance (IC) [17, 18], fuzzy logic controller (FLC) [19–21], sliding mode controller (SMC) [22, 23], particle swarm optimization (PSO) [24, 25], hysteresis controller (HC) [26], etc. The output voltages of the PV and PEMFC systems are given to the DC-DC boost converters to boost the voltage. Boost converter acts as front end power conditioning unit for renewable sources. The output from the DC link is given to the grid through an inverter.

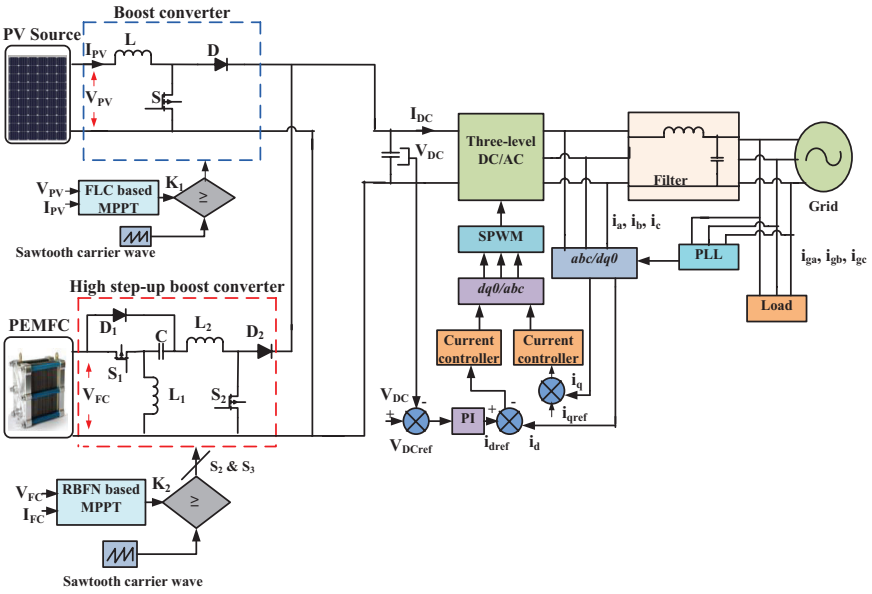

Figure 2 Proposed hybrid PV-PEMFC grid-connected system.

The proposed PV-PEMFC hybrid system is shown in Figure 2. In the proposed design a 950W BP Solar SX 3190 PV system and a 1.26kW PEMFC are used as input power sources. A conventional boost converter is used to boost the PV output voltage, whereas a high step-up DC-DC boost converter (HSBC) is designed for the PEMFC system to step-up the voltage. The designed HSBC reduces the voltage stress on power semiconductor switches and increases the efficiency of the PEMFC system. FLC and a radial basis function network (RBFN) based MPPT controllers are designed for the PV and PEMFC systems respectively to extract maximum power. The output voltage from these DC-DC converters is given to a 2kW, 230V, 50Hz AC grid system though a three-phase voltage source inverter (VSI). The three-phase VSI is controlled by using a current regulated controller.

The rest of the paper is organized as follows. The PV and PEMFC system modelings are discussed in Section 2. The design and analysis of conventional boost converter and HSBC are given in section 3. The FLC based MPPT controller for PV system and proposed RBFN based MPPT controller for PEMFC are discussed in Section 4. The simulation results for the proposed hybrid PV-PEMFC grid-connected systems are presented in Section 5 and the conclusions are summarized in Section 6.

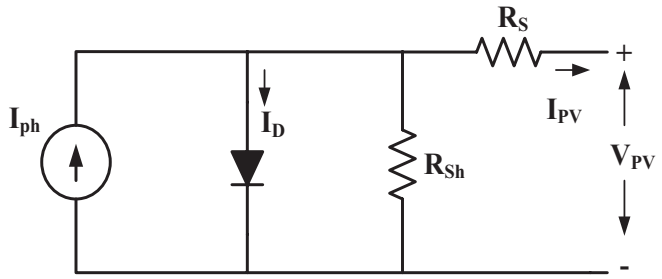

Figure 3 PV cell equivalent circuit.

2 Modeling of PV and Pemfc Systems

2.1 PV Cell Modeling

The equivalent circuit of the single diode model of a PV cell is shown in Figure 3. The circuit consists of a current source in parallel with a diode, series and shunt resistances. The mathematical model of the PV cell is derived by using the V-I characteristics PV system. The output voltage and current of the PV cell are given as follows [9, 27].

$$\mathrm{V}_{PV} = \frac{\eta \mathrm{KT}}{\mathrm{q}} \ln\left(\frac{\mathrm{I}_{ph}}{\mathrm{I}_{PV}} + 1\right) \tag{1}$$

$$\mathrm{I}_{PV} = \mathrm{I}_{ph} - \mathrm{I}_D \left[\exp\left(\frac{\mathrm{q}(\mathrm{V}_{PV} + \mathrm{R}_S \mathrm{I}_{PV})}{\eta \mathrm{KT}}\right) - 1\right] - \frac{\mathrm{V}_{PV} + \mathrm{R}_S \mathrm{I}_{PV}}{\mathrm{R}_{Sh}} \tag{2}$$

where V_{PV} is the PV output voltage, I_{ph} is PV cell phase current, I_{PV} is PV output current, I_D is diode saturation current, q is the charge of electron (1.698* 10^{-19}C), R_S and R_{Sh} are series and parallel resistances of the cell, K is Boltzmann constant (1.38*10^{-23} J/K), η ideality factor and T is absolute temperature of PV system.

The V-I and P-V characteristics of PV module at different irradiation levels of are shown in Figure 4. The output power of the PV cell depends on the irradiation value. If the irradiation is high then PV module will give maximum power otherwise vice versa. The proposed hybrid system is designed by considering a 950W BP solar SX3190 PV system and the simulation parameters of the same are listed in Table 1.

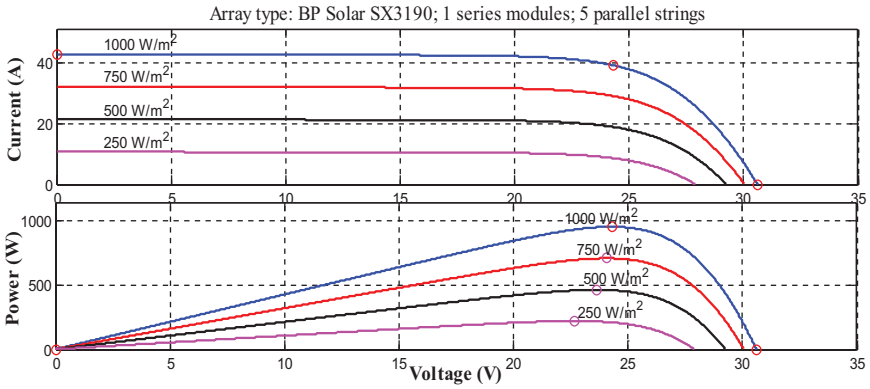

Figure 4 PV cell characteristics at different irradiation conditions.

Table 1 PV system Parameters

Description	Rating
Maximum Power (P_{max})	950 W
Maximum Voltage (V_{max})	24.3 V
Maximum Current (I_{max})	7.829 A
Open circuit Voltage (V_{OC})	30.6 V
Short circuit Current (I_{SC})	8.51 A
Irradiation (R)	600–1000 W/m^2
Temperature (T)	25°C
No. of PV cells connected in parallel	5

2.2 PEMFC Modeling

A PEMFC is an electrochemical energy conversion device, converts chemical energy of the fuel into electric energy. The schematic layout of the fuel cell is shown in Figure 5 [28]. It consists of a cathode, an anode and an electrolyte made with polymer electrolyte membrane. The operating principle of the PEMFC system is given as follows:

$$\begin{cases} 2H_2 \rightarrow 4H^+ + 4e^- \\ O_2 + 4H^+ + e^- \rightarrow 2H_2O \\ 2H_2 + O_2 \rightarrow 2H_2O + \text{energy} \end{cases} \tag{3}$$

A 1.26 kW PEMFC system is designed in MATLAB/Simulink for the proposed HRES. The electrical representation of PEMFC is shown in Figure 6.

The terminal voltage of the PEMFC stack is determined by using the Equation (4).

$$V_S = nV_{FC} \tag{4}$$

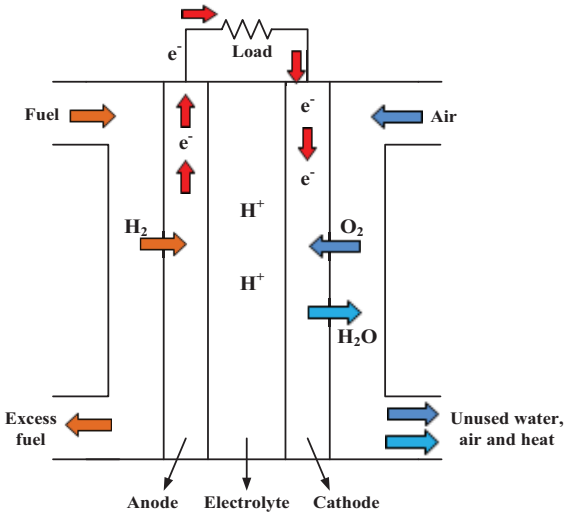

Figure 5 Schematic layout fuel cell.

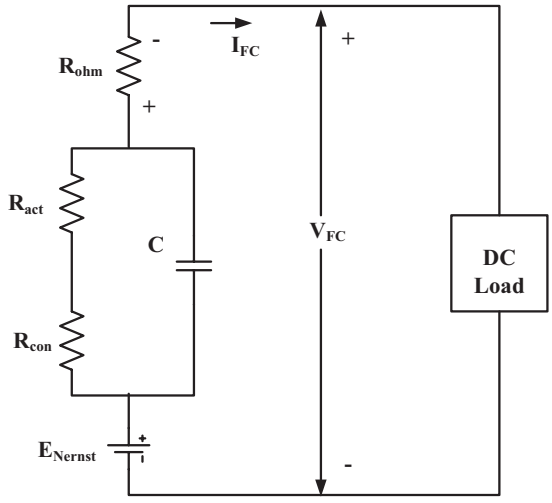

Figure 6 Electrical model of PEMFC.

where n is the number of PEMFC cells connected in series and V_{FC} is the output voltage of the single PEMFC cell.

$$V_{FC} = E_{Nernst} - V_{ohm} - V_{act} - V_{con} \tag{5}$$

where E_{nernst} is open circuit thermodynamic voltage; V_{ohm} is activation overvoltage; V_{act} is activation overvoltage; V_{con} is concentration voltage.

Each term in Equation (5) are determined by using the following expressions [29–31]:

$$\begin{aligned} \mathrm{E}_{Nernst} = 1.229 - 8.5\mathrm{e}^{-4}\left(\mathrm{T}_{FC} - 298.15\right) \\ + 4.308\mathrm{e}^{-5}\left[\ln\left(\mathrm{P}_{H2}\right) + 0.5\ln\left(\mathrm{P}_{O2}\right)\right] \end{aligned} \tag{6}$$

$$\mathrm{V}_{ohm} = \mathrm{R}_{FC}.\mathrm{I}_{FC} \tag{7}$$

$$\mathrm{V}_{act} = \mathrm{T}_{FC}\left(\mathrm{x} + \mathrm{y}\ln\left(\mathrm{I}_{FC}\right)\right) \tag{8}$$

$$\mathrm{V}_{con} = -0.016\ln\left(1 - \frac{\mathrm{I}_{FC}}{25}\right) \tag{9}$$

where T_{FC} is PEMFC temperature, I_{FC} is PEMFC current, P_{H2} is hydrogen gas partial pressure, P_{O2} is oxygen gas partial pressure, x and y are constants. The V-I characteristics of the PEMFC are shown in Figure 7. The design specifications of 1.26kW PEMFC are listed in Table 2.

3 Design of DC-DC Boost Converters

Boost converter acts as front end power conditioning unit for renewable sources. To maintain voltage stability at the DC link, two different types of DC-DC boost converters are used in the proposed hybrid system. A conventional boost converter is used for the PV system and a high step-up boost converter is designed for PEMFC system.

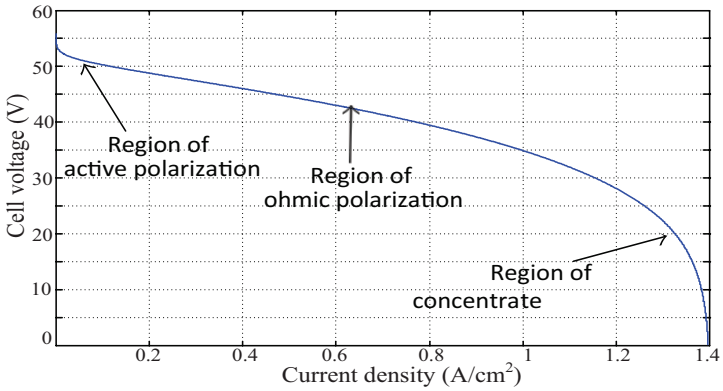

Figure 7 V-I characteristics of PEMFC.

Table 2 PEMFC specifications

Parameter	Value
Maximum power (W)	1260
Maximum voltage (V)	24.23
Maximum current (A)	52
Number of cells	42
Nominal fuel flow rate (lpm)	417.3
Nominal air flow rate (lpm)	2400
Hydrogen partial pressure (bar)	1.5
Oxygen partial pressure (bar)	1

3.1 Conventional Boost Converter

The output of the PV source is given to the conventional DC-DC boost converter to boost the PV output voltage. The boost converter consists of an inductor (L), a switch (S), a diode (D) and a capacitor (C) as shown in Figure 8.

When the switch S is switched ON, the diode D is in reverse bias condition. In this case, inductor L gets charged from the supply voltage. The voltage across the inductor L is given as follows.

$$V_L = V_{PV} \tag{10}$$

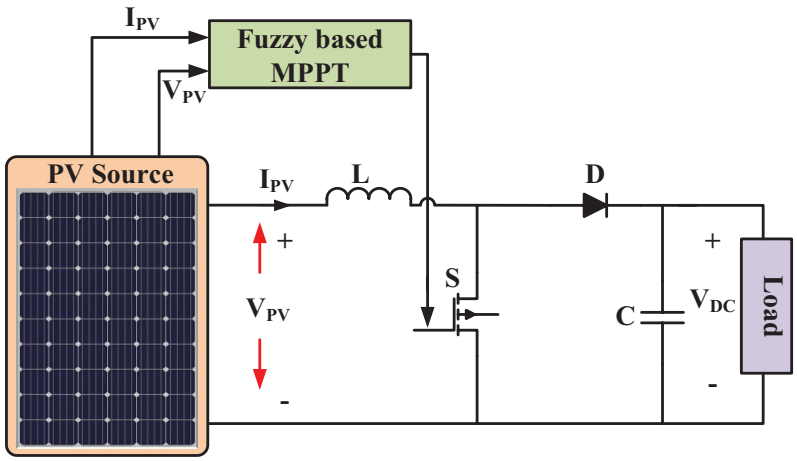

Figure 8 conventional boost converters with PV system.

When the switch S is switched OFF, the diode D is in forward bias condition. In this case, inductor L gets discharged through the load. The voltage across the inductor L is given as

$$V_L = V_{PV} - V_{DC} \tag{11}$$

According to volt-second balance condition, the average voltage across an inductor is zero. By applying volt-second balance on inductor L, we get

$$V_{PV} . K_1 + (V_{PV} - V_{DC}) . (1 - K_1) \; = \; 0 \tag{12}$$

From Equation (12), the static voltage gain of the conventional boost converter is obtained as

$$M_1 = \frac{V_{DC}}{V_{PV}} = \frac{1}{1 - K_1} \tag{13}$$

The values of the inductor L and capacitor C are calculated by using the following equations.

$$L = \frac{V_{FC} K_1 T_S}{\Delta I_L} \tag{14}$$

$$C = \frac{I_{DC} K_1 T_S}{\Delta V_{DC}} \tag{15}$$

3.2 High Step-up Boost Converter (HSBC)

The circuit topology of the HSBC is shown in Figure 9. The HSBC has two switches ($S_1$and S_2), two diodes (D_1 and D_2), two inductors (L_1 and L_2) and two capacitors (C and C_0). The gate pulses are given to the two switches S_1 and S_2 simultaneously.

When both the switches S_1 and S_2 are switched ON, the diodes D_1 and D_2 are in reverse bias. During this period, the input voltage source V_{FC} charges both the inductors L_1 and $L_2$and the capacitor C_0 supplies the energy to the load. In this state, the voltages across the inductors L_1 and L_2 are given as follows.

$$V_{L1} \; = \; V_{FC} \tag{16}$$

$$V_{L2} \; = \; (V_{FC} - V_C) \tag{17}$$

When the switches S_1 and S_2 are switched OFF, the diodes D_1 and D_2 are in forward bias. During this time, the current through both the inductors decreases linearly. The voltages across the inductors L_1 and L_2 are given as follows.

$$V_{L1} \; = \; V_{FC} + V_C \tag{18}$$

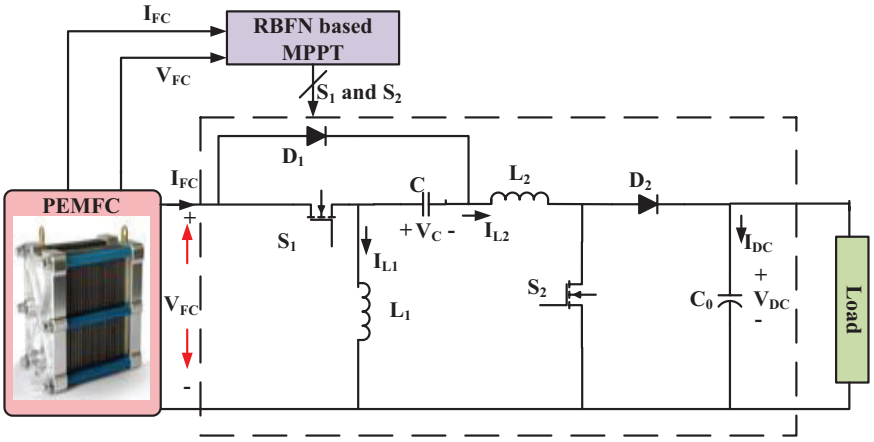

Figure 9 High step-up boost converter with PEMFC.

$$V_{L2} = V_{FC} - V_{DC} \tag{19}$$

The static voltage gain (M_2) of the HSBC is obtained by employing volt-second balance principle on both inductors. Now by employing volt-second balance principle on the inductor L_1, we get

$$\int_0^{K_2 T_S} (V_{FC})\, dt + \int_{K_2 T_S}^{T_S} (V_{FC} + V_C)\, dt = 0 \tag{20}$$

From Equation (20), the capacitor voltage V_C is obtained as,

$$V_C = \frac{-V_{FC}}{1} - K_2 \tag{21}$$

where K_2 is duty cycle of the HSBC. Similarly, by employing volt-second balance principle on the inductor L_2, we get

$$\int_0^{K_2 T_S} (V_{FC} - V_C)\, dt + \int_{K_2 T_S}^{T_S} (\mathrm{V}_{FC} - V_{DC})\, dt = 0 \tag{22}$$

From Equations (21) and (22), the static voltage gain M_2 of the designed HSBC is obtained as

$$\mathrm{M}_2 = \frac{\mathrm{V}_{DC}}{\mathrm{V}_{FC}} = \frac{1}{(1 - \mathrm{K}_2)^2} \tag{23}$$

The values of the inductors L_1 and L_2 are calculated by using the inductors current ripples (ΔI_{L1}, ΔI_{L2}) and the voltage across the inductors.

$$L_1 = \frac{K_2 V_{FC} T_S}{2\Delta I_{L1}} \tag{24}$$

$$L_2 = \frac{K_2 \mathrm{V}_{FC} T_S}{2\Delta\, I_{L2}} \left(1 + \frac{1}{1 - K_2}\right) \tag{25}$$

The values of the capacitors C and C_0 are calculated by using the capacitors voltage ripples (ΔV_{C1}, ΔV_{C0}) and the current through the capacitors.

$$C_1 = \frac{K_2 V_{DC} T_S}{2\Delta\, \mathrm{V}_{C1} (1 - K_2)} \tag{26}$$

$$C_0 = \frac{K_2 V_{DC} T_S}{2\Delta\, V_{C0}} \tag{27}$$

4 Design of MPPT Controllers

In order to increase the efficiency of the hybrid system, MPPT controllers are necessary for both PV and PEMFC systems. The maximum power point of the PV system depends on solar irradiation levels. Whereas the maximum power point of the PEMFC changes with respect to change in cell temperature and change in hydrogen or oxygen gas partial pressures. In this paper, a fuzzy logic based MPPT controller is used for PV system and RBFN based MPPT controller is designed for PEMFC system.

4.1 FLC Based MPPT Controller for PV System

FLC is a rule-based technique and is operated by using membership functions. Exact mathematical model of the system is not required in case of FLC. FLC has the advantages of easy operation, fast response and user-friendly interface [32]. The architecture of FLC consists of fuzzification, inference engine, rule base and defuzzification as shown in Figure 10 [33]. The input variables to the FLC are error (E) and change in error (ΔE) and the output variable is change in duty cycle (ΔK). The error (E) is set as the change in power of the PEMFC with respect to change in voltage and is given as,

$$E(n) = \frac{P_{PV}(n) - P_{PV}(n-1)}{V_{PV}(n) - V_{PV}(n-1)} \tag{28}$$

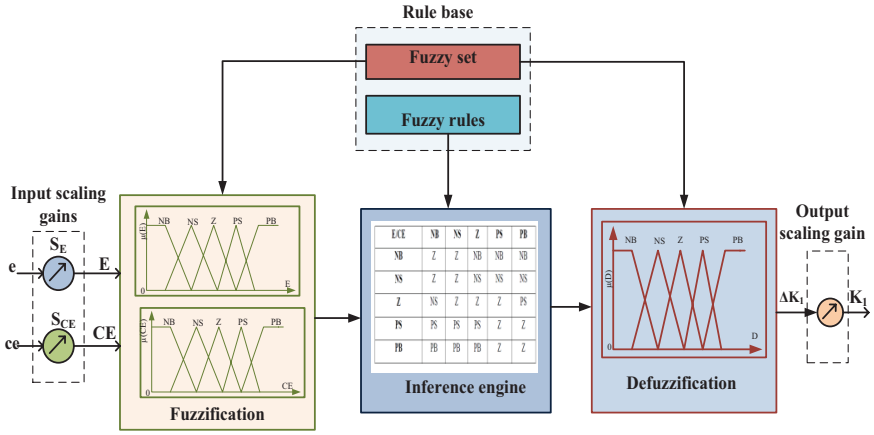

Figure 10 Structure of FLC.

the change in error is given as,

$$\Delta E = E(n) - E(n-1) \tag{29}$$

where $P_{PV}(n)$ and $V_{PV}(n)$ are instant power and voltage of the PV system.

During the fuzzification process, the input variables V_{FC} and I_{FC} are converted into linguistic functions depending on the type of membership function chosen. In the inference engine, the linguistic functions are manipulated by using the rules in the rule base. In defuzzification stage, the linguistic parameters are converted into a numerical value by using the membership functions [34]. The membership functions are designed by using Mamdani's method. The applied inference rules are listed in Table 3.

Table 3 Fuzzy inference rules

E	**ΔE**				
	NH	**NL**	**Z**	**PL**	**PH**
NH	Z	Z	NL	NL	NL
NL	Z	Z	NH	NH	NH
Z	NH	Z	Z	Z	PH
PL	PH	PH	PH	Z	Z
PH	PL	PL	PL	Z	Z

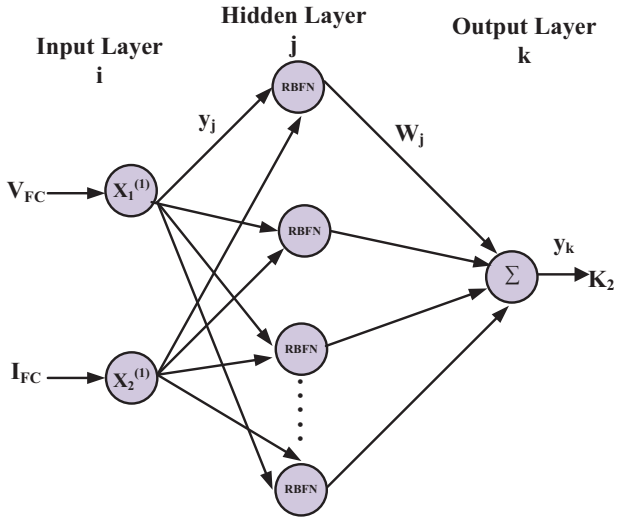

Figure 11 Structure of RBFN.

4.2 RBFN Based MPPT Controller for PEMFC

RBFN is a feed-forward neural network model which has both supervised and unsupervised learning phases. RBFN typically consists of three layers: an input layer, a hidden layer and an output layer as shown in Figure 11. The hidden layer consists of non-linear radial basis activation function whereas the output layer is linear one [35, 36]. The training process of the RBFN is accomplished in two steps. First, the unsupervised training method is executed and the input parameters are controlled by the radial basis functions. In the next step, the supervised training method is implemented to train the weights which are same as the backpropagation training algorithm. In this paper, the inputs to the RBFN controller are voltage and current from the PEMFC and the output is control signal (K_2) which is given to the high step-up boost converter to control the output voltage.

The input layer of RBFN has two neurons to transmit the data to the next layer. The net input and the net output of the input layer are given as,

$$x_i^{(1)}(n) \;=\; net_i^{(1)} \tag{30}$$

$$y_i^{(1)}(n) \;=\; f_i^{(1)}[net_i^{(1)}(n)] \;=\; net_i^{(1)}(n),\; i = 1, 2 \tag{31}$$

where is input layer, y_i^1 is hidden layer and net_i^1 is sum of the input layer. Every node in the hidden layer performs a Gaussian function. The Gaussian function is used as a membership function in the RBFN.

$$net_j^{(2)}(n) \;=\; -(X - M_j)^T \sum_j (X - M_j) \tag{32}$$

$$y_j^{(2)}(n) \;=\; f_j^{(2)}\left[net_j^{(2)}(n)\right] exp[net_j^{(2)}(n)]\,,\; j = 1, 2, ... \tag{33}$$

where M_j and $\sum j$ are mean and standard deviation of the Gaussian function respectively. The output layer has single node t, generates the linear control signal (K_2).

$$net_t^{(3)} \;=\; \sum_j w_j y_j^{(2)} \tag{34}$$

$$y_t^{(3)} \;=\; f_t^{(3)}\left[net_t^{(3)}(n)\right] \;=\; net_t^{(3)}(n) \tag{35}$$

where w_j is the connective weight matrix between the output and hidden layer.

After initialization RBFN, a supervised training algorithm is executed to train the system. This training process is similar to the backpropagation algorithm. It is hired to tune the parameters of the RBFN by using training patterns. The error of each layer in RBFN is determined and updated by supervised training algorithm. The error of the system E is expressed as,

$$E = \sum \frac{1}{2}\left(V_{DC} - V_{MPP}\right) \tag{36}$$

where V_{DC} is reference or pre-defined output voltage and V_{MPP} is actual or obtained output voltage. Figure 12 shows the RBFN MPPT controller for PEMFC system. PEMFC temperature and current are the input variables to the RBFN controller and the output variable is duty cycle. Figure 13 shows the designed RBFN controller in the MATLAB/Simulink and the optimal configuration parameters chosen for the RBFN controller are listed in Table 4.

5 Results and Discussions

The proposed hybrid PV-PEMFC grid-connected system is designed and simulated for a load demand of 800VAR reactive and 2000W active powers. The output power of the DC link is given to the three phase VSI and its control system is shown in Figure 1. The obtained i_q and V_{DC} are compared with i_{qref} and V_{DCref} respectively and the error values are fed to the PI controller

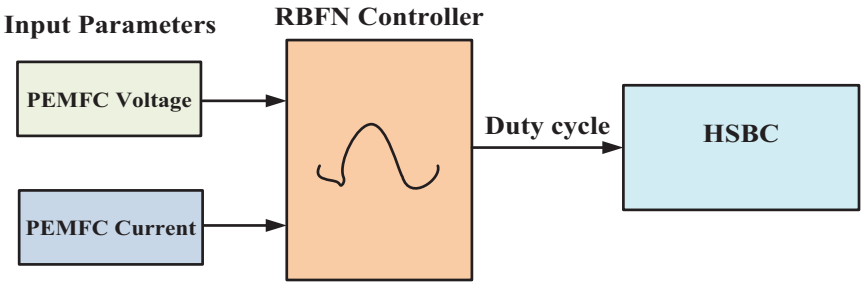

Figure 12 Designed RBFN controller in MATLAB/Simulink.

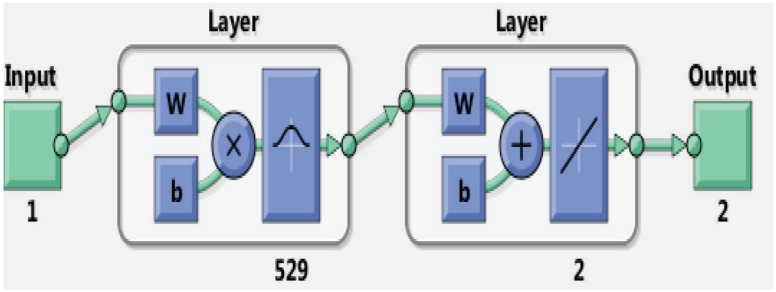

Figure 13 Designed RBFN controller in MATLAB/Simulink.

Table 4 Optimal configuration parameters of RBFN

Parameter	Value/method
Input variable	V_{FC}, I_{FC}
Output variable	Duty cycle
Maximum limit of hidden neurons	529
Spread factor	0.01
Training algorithm	OLS

to generate control gate pulses. The specifications of the PV and PEMFC systems are given in Table 1 and Table 2 respectively.

To analyze the dynamic response of the proposed hybrid system, sudden changes in PV irradiation levels and PEMFC temperatures are considered. Different solar PV irradiation levels are given as follows: at first from 0 to 0.3s is 800 W/m^2, from 0.3 to 0.6s is 600 W/m^{2}and from 0.6 to 0.9s is given as 1000 W/m^{2}as shown in Figure 14. The considered PEMFC temperatures are T=320K for a time period of 0 to 0.3sec, T=300K for 0.3 sec to 0.6sec and T=340K for a period of 0.6sec to 0.9sec as shown in Figure 15.

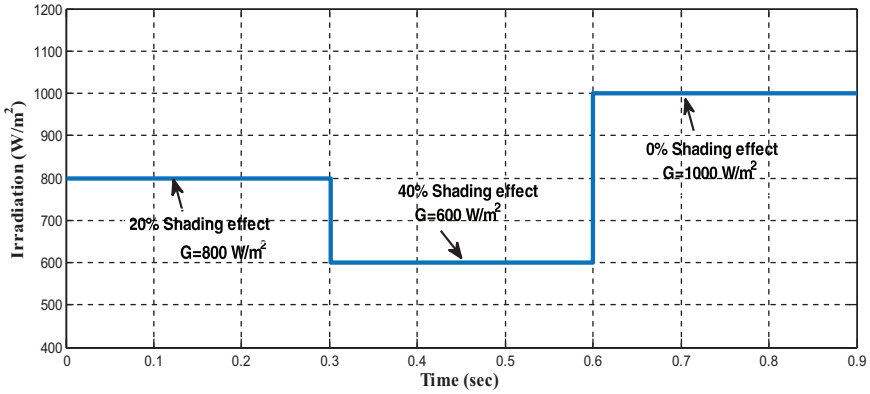

Figure 14 Considered solar irradiation for PV system.

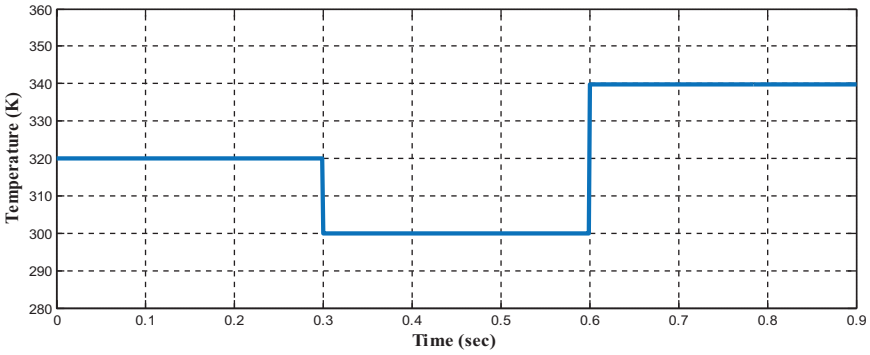

Figure 15 Considered temperature changes for PEMFC system.

For the considered irradiations the output current, voltage and power waveforms of BP Solar SX 3190 PV module are as shown in Figure 16. It generates a power of 685W for 0 to 0.3 sec, 465W for 0.3sec to 0.6 sec and 940W for 0.6sec to 0.9sec. Figure 17 shows the PEMFC output current, voltage and power waveforms for the considered temperatures. The PEMFC generates a power of 820W for a time period of 0 to 0.3sec, 630W for 0.3sec o 0.9sec and 1210W from 0.6sec to 0.9sec. The load, inverter and grid side current and voltage waveforms are shown in Figure 18 to Figure 20.

The active power profile of the load, inverter and grid side of the proposed hybrid system is shown in Figure 21. For 0 to 0.3sec period the load demand of 2000W is satisfied by both hybrid and grid sources with 1500W and 490W respectively, similarly, for 0.3sec to 0.6sec the hybrid PV-PEMFC contribution is 1090W and grid contribution is 900W and for 0.6sec to 0.9sec the hybrid

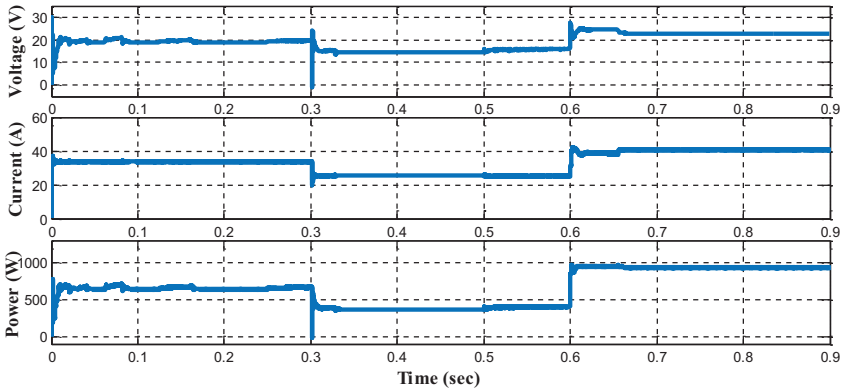

Figure 16 PV system output voltage, current and power at different irradiations.

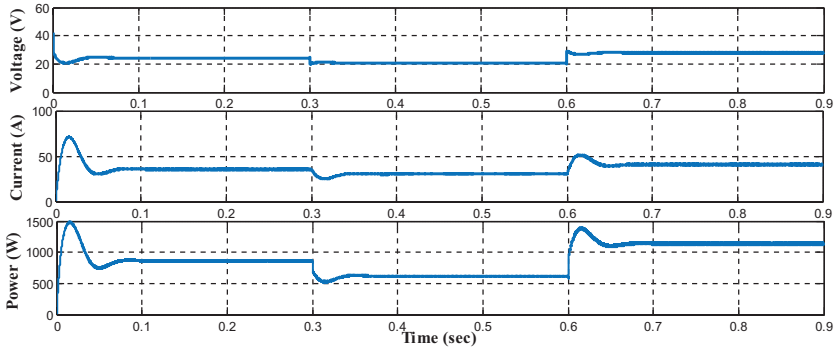

Figure 17 PEMFC output voltage, current and power at different temperatures.

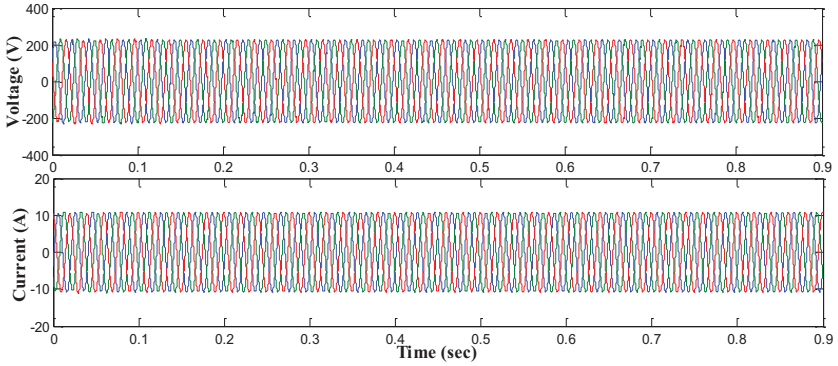

Figure 18 Load current and voltage waveforms.

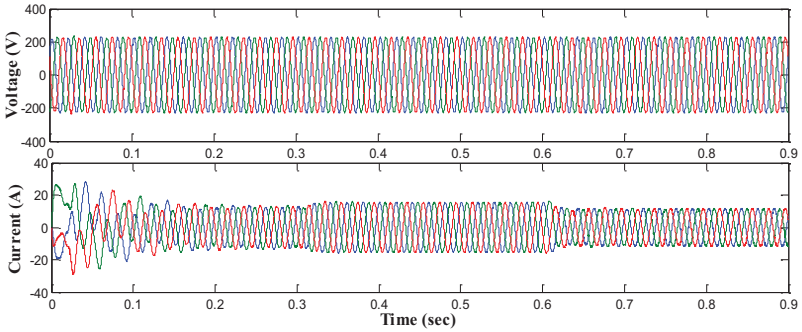

Figure 19 Inverter current and voltage waveforms.

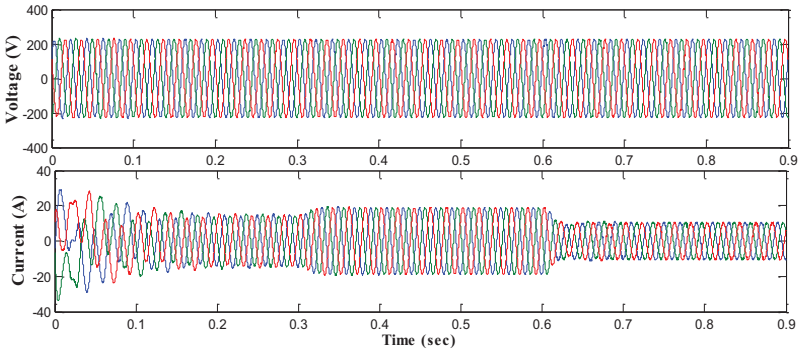

Figure 20 Grid current and voltage waveforms.

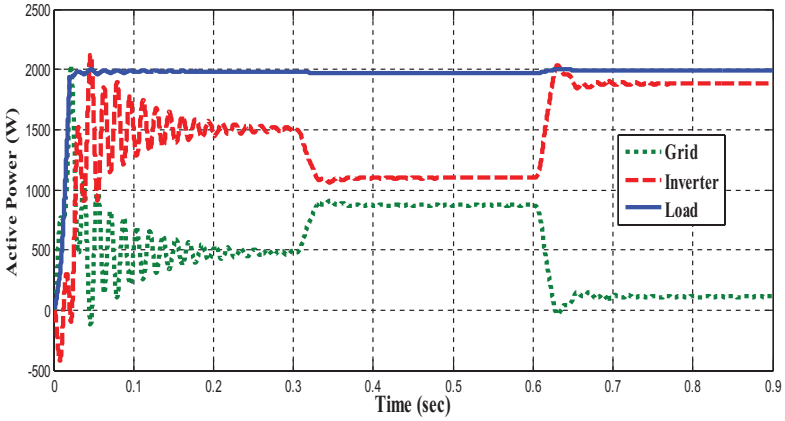

Figure 21 Active power output of the load, inverter and grid.

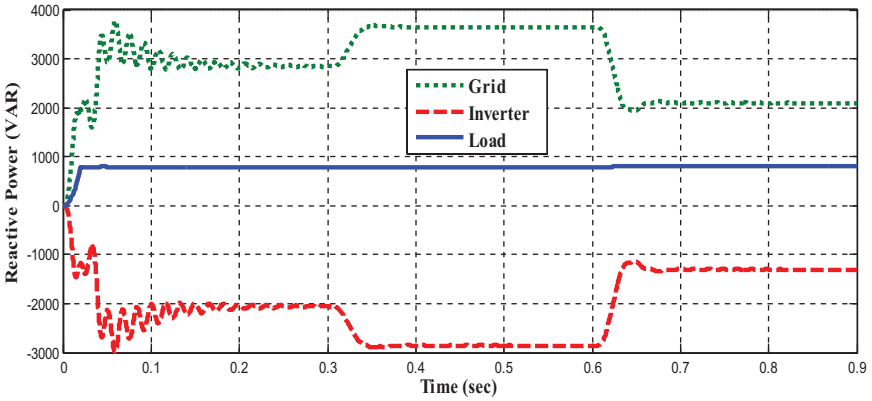

Figure 22 Reactive power output of the load, inverter and grid.

Table 5 Analysis active and reactive powers

Parameter	Active Power (W)			Reactive Power (VAR)		
Time period (sec)	0 to 0.3	0.3 to 0.6	0.6 to 0.9	0 to 0.3	0.3 to 0.6	0.6 to 0.9
Load output (W)	1990	1990	1990	795	795	795
Inverter output (W)	1500	1090	1880	–2135	–2935	–1255
Grid output (W)	490	900	110	2930	3730	2050

contribution is 1880W and grid source offers 110W active power. Similarly, Figure 22 shows the reactive power profile of load, inverter and grid side of the PEMFC system. The assumed reactive power of 800VAR is generated by both hybrid PV-PEMFC systems and grid for the considered time intervals. The complete analysis of the active and reactive power profile grid connected PEMFC system is given in Table 5.

6 Conclusion

In this paper, a three-phase grid connected hybrid renewable energy system is designed with 950W solar PV and 1.26kW PEMFC. A new RBFN based MPPT controller is proposed for the PEMFC system and FLC MPPT controller is used for the PV system. The designed MPPT controllers have effectively extracted the maximum power from the PV and PEMFC systems at different solar

irradiation levels and cell temperatures respectively. Furthermore, a high step-up boost converter is designed for the PEMFC system to provide high step-up voltage. As future work, we plan to analyze the proposed hybrid PV-PEMFC system by using the experimental platform.

References

[1] Saad, N. H., El-Sattar, A. A., and Mansour, A. E. A. M. (2017). A novel control strategy for grid connected hybrid renewable energy systems using improved particle swarm optimization. *Ain Shams Engineering Journal*.

[2] Reddy, S. S. (2017). Optimization of Renewable Energy Resources in Hybrid Energy Systems. *Journal of Green Engineering,* 7(1), 43–60.

[3] Rajkumar, R. K., Ramachandaramurthy, V. K., Yong, B. L., and Chia, D. B. (2011). Techno-economical optimization of hybrid pv/wind/battery system using Neuro-Fuzzy. *Energy,* 36(8), 5148–5153.

[4] Arul, P. G., Ramachandaramurthy, V. K., and Rajkumar, R. K. (2015). Control strategies for a hybrid renewable energy system: A review. *Renewable and Sustainable Energy Reviews,* 42, 597–608.

[5] Basaran, K., Cetin, N. S., and Borekci, S. (2016). Energy management for on-grid and off-grid wind/PV and battery hybrid systems. *IET Renewable Power Generation,* 11(5), 642–649.

[6] Caballero, F., Sauma, E., and Yanine, F. (2013). Business optimal design of a grid-connected hybrid PV (photovoltaic)-wind energy system without energy storage for an Easter Island's block. *Energy,* 61, 248–261.

[7] Behravesh, V., Keypour, R., and Foroud, A. A. (2018). Stochastic analysis of solar and wind hybrid rooftop generation systems and their impact on voltage behavior in low voltage distribution systems. *Solar Energy,* 166, 317–333.

[8] Kumar, K., Babu, N. R., and Prabhu, K. R. (2017). Design and Analysis of RBFN-Based Single MPPT Controller for Hybrid Solar and Wind Energy System. *IEEE Access, 5*, 15308–15317.

[9] Kumar, K., Babu, N. R., and Prabhu, K. R. (2017). Design and analysis of an integrated Cuk-SEPIC converter with MPPT for standalone wind/PV hybrid system. *International Journal of Renewable Energy Research (IJRER),* 7(1), 96–106.

[10] Thounthong, P., Chunkag, V., Sethakul, P., Sikkabut, S., Pierfederici, S., and Davat, B. (2011). Energy management

of fuel cell/solar cell/supercapacitor hybrid power source. *Journal of power sources,* 196(1), 313–324.

[11] Thounthong, P., Luksanasakul, A., Koseeyaporn, P., and Davat, B. (2013). Intelligent model-based control of a standalone photovoltaic/fuel cell power plant with supercapacitor energy storage. *IEEE Transactions on Sustainable Energy,* 4(1), 240–249.

[12] Mebarki, N., Rekioua, T., Mokrani, Z., Rekioua, D., and Bacha, S. (2016). PEM fuel cell/battery storage system supplying electric vehicle. *International Journal of Hydrogen Energy,* 41(45), 20993–21005.

[13] García, P., García, C. A., Fernández, L. M., Llorens, F., and Jurado, F. (2014). ANFIS-based control of a grid-connected hybrid system integrating renewable energies, hydrogen and batteries. *IEEE Transactions on industrial informatics,* 10(2), 1107–1117.

[14] Reddy, K. J., and Sudhakar, N. (2018). High Voltage Gain Interleaved Boost Converter With Neural Network Based MPPT Controller for Fuel Cell Based Electric Vehicle Applications. *IEEE Access,* 6, 3899–3908.

[15] De Brito, M. A. G., Galotto, L., Sampaio, L. P., e Melo, G. D. A., and Canesin, C. A. (2013). Evaluation of the main MPPT techniques for photovoltaic applications. *IEEE transactions on industrial electronics,* 60(3), 1156–1167.

[16] Kiruthiga, K., Dyaneswaran, A., Kavitha, B., and Prakash, R. A. (2014). Grid connected hybrid fuel cell-PO based MPPT for partially shaded solar PV system. *Int J P2P Netw Trends Technol,* 7, 29–33.

[17] Tey, K. S., and Mekhilef, S. (2014). Modified incremental conductance MPPT algorithm to mitigate inaccurate responses under fast-changing solar irradiation level. *Solar Energy,* 101, 333–342.

[18] Harrag, A., and Bahri, H. (2016). IC-based variable step size MPPT controller for PEMFC power system-analysis and performance improvements. In *Proceedings International Symposium on Sustainable Hydrogen (ISSH2'2016), Alger, Algeria*.

[19] Ozdemir, S., Altin, N., and Sefa, I. (2017). Fuzzy logic based MPPT controller for high conversion ratio quadratic boost converter. *International Journal of Hydrogen Energy*, 42(28), 17748–17759.

[20] Sekhar, V. (2016). Modified Fuzzy Logic Based Control Strategy for Grid Connected Wind Energy Conversion System. *Journal of Green Engineering,* 6(4), 369–384.

[21] Harrag, A., and Messalti, S. (2018). How fuzzy logic can improve PEM fuel cell MPPT performances. *International Journal of Hydrogen Energy,* 43(1), 537–550.

[22] Kchaou, A., Naamane, A., Koubaa, Y., and M'sirdi, N. (2017). Second order sliding mode-based MPPT control for photovoltaic applications. *Solar Energy,* 155, 758–769.

[23] Hahm, J., Kang, H., Baek, J., Lee, H., and Park, M. (2015). Design of incremental conductance sliding mode MPPT control applied by integrated photovoltaic and proton exchange membrane fuel cell system under various operating conditions for BLDC motor. *International Journal of Photoenergy,* 2015.

[24] da Silva, S. A. O., Sampaio, L. P., de Oliveira, F. M., and Durand, F. R. (2016). Feed-forward DC-bus control loop applied to a single-phase grid-connected PV system operating with PSO-based MPPT technique and active power-line conditioning. *IET Renewable Power Generation,* 11(1), 183–193.

[25] Ahmadi, S., Abdi, S., and Kakavand, M. (2017). Maximum power point tracking of a proton exchange membrane fuel cell system using PSO-PID controller. *International Journal of Hydrogen Energy,* 42(32), 20430–20443.

[26] Park, J. D., and Ren, Z. (2012). Hysteresis controller based maximum power point tracking energy harvesting system for microbial fuel cells. *Journal of Power Sources,* 205, 151–156.

[27] Hong, C. M., and Chen, C. H. (2014). Intelligent control of a grid-connected wind-photovoltaic hybrid power systems. *International Journal of Electrical Power & Energy Systems,* 55, 554–561.

[28] Arya, S. R., and Kumar, N. S. (2017). Grid Connected Fuel Cell Based Distributed Power Generation System. *Journal of Green Engineering,* 7(1), 285–310.

[29] Benyahia, N., Denoun, H., Zaouia, M., Rekioua, T., and Benamrouche, N. (2015). Power system simulation of fuel cell and supercapacitor based electric vehicle using an interleaving technique. *International Journal of Hydrogen Energy,* 40(45), 15806–15814.

[30] Allaoua, B., Draoui, B., and Belatrache, D. (2017). Study of the energy performance of a PEM fuel cell vehicle. *International Journal of Renewable Energy Research (IJRER),* 7(3), 1395–1402.

[31] Gong, W., and Cai, Z. (2013). Accelerating parameter identification of proton exchange membrane fuel cell model with ranking-based differential evolution. *Energy*, 59, 356–364.

[32] Tiwari, R., and Babu, N. R. (2016). Recent developments of control strategies for wind energy conversion system. *Renewable and Sustainable Energy Reviews,* 66, 268–285.

[33] Bendib, B., Krim, F., Belmili, H., Almi, M. F., and Boulouma, S. (2014). Advanced Fuzzy MPPT Controller for a stand-alone PV system. *Energy Procedia,* 50, 383–392.

[34] Saravanan, S., and Babu, N. R. (2016). Maximum power point tracking algorithms for photovoltaic system–A review. *Renewable and Sustainable Energy Reviews,* 57, 192–204.

[35] Saravanan, S., and Babu, N. R. (2016). RBFN based MPPT algorithm for PV system with high step up converter. *Energy conversion and Management,* 122, 239–251.

[36] Tiwari, R., Padmanaban, S., and Neelakandan, R. B. (2017). Coordinated Control Strategies for a Permanent Magnet Synchronous Generator Based Wind Energy Conversion System. *Energies*, 10(10), 1493.

Biographies

Jyotheeswara Reddy K. received the B.Tech. degree in Electrical and Electronics Engineering from JNTU-Kakinada in 2012 and M.E degree in Power Electronics and Industrial Drives from Sathyabama University in 2014. He is currently pursuing the Ph.D degree with Vellore Institute of Technology, Vellore. His research work focused in the field of power electronic applications in the renewable energy systems.

Sudhakar N. received the B.E degree in Electrical and Electronics Engineering from Bharathiyar University, the M.Tech. degree in Elecrical Drives and Control from Pondicherry University, and the Ph.D degree from VIT University. He is currently working as Associate Professor in School of Electrical Engineering, Vellore Institute of Technology, Vellore. His research work focused in the area of EMI/EMC in power converters and Electric Vehicles.